Fundamentals of Vapor Phase Epitaxial Growth Processes

G. B. Stringfellow

Citation: AIP Conf. Proc. **916**, 48 (2007); doi: 10.1063/1.2751909
View online: http://dx.doi.org/10.1063/1.2751909
View Table of Contents: http://proceedings.aip.org/dbt/dbt.jsp?KEY=APCPCS&Volume=916&Issue=1
Published by the American Institute of Physics.

Fundamentals of Vapor Phase Epitaxial Growth Processes

G. B. Stringfellow

Department of Materials Science and Engineering
University of Utah
Salt Lake City, UT 84112

Abstract.. The first success with the growth of semiconductor materials by vapor phase epitaxy (VPE) dates back to the 1950's. Today, it is the largest volume technique for the production of both Si and III/V electronic and photonic devices. Of course, commercial processes for the growth of Si layers, dielectrics, and metals are part of a multi-billion dollar industry. Even for the III/V semiconductors commercial reactors can be purchased yielding 2000 cm^2/run, mainly for the production of light emitting diodes and solar cells.The various vapor phase epitaxial processes share a basic underpinning of thermodynamics and kinetics. The vehicle used for this paper will be mainly the organometallic growth of III/V materials. It will briefly discuss key concepts in our understanding of the complex growth process, including both kinetic and thermodynamic aspects of vapor growth. Special attention will be paid to surface processes and the use of surfactants to control the properties of the resulting materials. Our understanding of this topic is still developing rapidly.

Keywords: OMVPE, thermodynamics, epitaxy.
PACS: 81.05.Bx, 81.10.Bk, 81.15Gh, 81.15kk, 82.33.Ya

INTRODUCTION

Today, many semiconductor devices and circuits require vapor phase epitaxial growth processes. For compound semiconductors, nearly all devices have always required epitaxy due to the use of alloys, the extremely high quality needed for minority carrier devices and the fine geometries required, especially now when bandgap engineered structures require quantum wells, wires, and dots. A number of vapor phase epitaxial growth techniques have been developed for the semiconductor industry over the last 50 years. The earliest processes used halides and hydrides for transporting the constituents for both Si and IIII/V semiconductors. However, in recent years these techniques have been largely displaced by more flexible techniques for the growth of a wide range of materials and special structures. These include organometallic vapor phase epitaxy [OMVPE, or equivalently MOVPE, MOCVD or OMCVD, molecular beam epitaxy (MBE), and chemical beam epitaxy (CBE)]. OMVPE has come to be the leading technique for the production of III/V materials, especially for solar cells and light emitting diodes (LEDs). Thus, it is used for the commercial scale production of AlGaInP alloys for visible LEDs, injection lasers, and

CP916, *Perspectives on Inorganic, Organic, and Biological Crystal Growth: From Fundamentals to Applications, 13th International Summer School on Crystal Growth*
edited by M. Skowronski, J. J. DeYoreo, and C. A. Wang

solar cells and for AlGaInN alloys for green LEDs and blue injection lasers and LEDs. Today, commercially available reactors can be purchased for both laboratory-scale and large production-scale applications from several manufacturers. For an in-depth reviw of the OMVPE technique see Ref. [1].

MBE has, for decades, been the leading technique for the production of fine-scale structures. It was the first technique to produce layers showing quantum confinement and has been at the forefront of the development of bandgap engineered structures. Reviews and books are available for in-depth reviews of the technique and applications [2-4].

CBE is essentially a hybrid of OMVPE and MBE. It uses an ultra-high vacuum chamber, as for MBE, but uses organometallic or hydride precursors, rather than the elemental sources used in MBE. This gives certain advantages, but this technique remains mainly a laboratory technique, which is used less frequently than OMVPE and MBE in production operations.

Each of these vapor phase epitaxial growth processes is exquisitely complex when viewed in detail at the atomic level. As a result, even after many thousands of man years of effort, we are still nowhere near a complete understanding. Indeed, early crystal growth studies were largely empirical, giving epitaxy the appearance of an art. This is partly because of the complex, multicomponent, multiphase systems that are normally of interest and partly because the process is dynamic and inhomogeneous phases are inherent. In an effort to systematically study and understand such a complex system the fundamental processes occurring during epitaxial growth are commonly subdivided into hydrodynamics and mass transport, the kinetics of chemical reactions occurring homogeneously in the gas phase and heterogeneously at the surface, and thermodynamics. We will concentrate on thermodynamics in this paper, using specific cases of OMVPE growth of III/V semiconductors as examples. The hydrodynamic and kinetic aspects of OMVPE will be addressed briefly, but detailed discussions of both topics can be found in the literature [1,5]. Increasingly, an understanding of the basic aspects of epitaxy has allowed a departure from the empirical approach to crystal growth.

Thermodynamic aspects of vapor phase epitaxial growth are in many ways the most basic. This is especially true for the very slow growth rates typically used for semiconductor epitaxy. At low growth rates and relatively high temperatures, the chemical reaction kinetics play less of a role than in very rapid crystal growth processes. In the limit of infinitely slow growth rates thermodynamics defines the concentrations of all species in the vapor and solid phases. So thermodynamics can be used to predict solid composition for many growth conditions. This includes not only alloy composition, but also solid stoichiometry, incorporation of impurities, separation into several solid phases, and the spontaneous occurrence of ordered superlattice structures in the solid. Thermodynamics also determines the driving force for any crystal growth process, hence defining the maximum growth rate. Thus, the thermodynamic aspects of epitaxy must be understood before considering the kinetic aspects of growth that frequently control growth rate and, in many situations, affect solid composition and microstructure for semiconductor alloys [2,3]. However, it is often vital to include the thermodynamics of the surface in order to understand the

microstructure, particularly for semiconductor alloys. The effort to control surface thermodynamics has recently led to the use of surfactants during VPE growth.

Thermodynamic Treatment of VPE

The equilibrium state for a two phase, $\alpha+\beta$, system is defined in terms of the chemical potentials,

$$\mu_i^{\alpha} = \mu_i^{\beta} \ , \tag{1}$$

where the subscript i indicates the ith component and the superscripts indicate the phase. The chemical potential is usually written in terms of the chemical potential in an arbitrary standard state, denoted by the superscript zero,

$$\mu = \mu^o + RT \ln\left(p / p_o\right) \ . \tag{2}$$

For an ideal gas mixture,

$$\mu_i = \mu_i^o + RT \ln\left(p_i / p_i^o\right), \tag{3}$$

where p_i is the partial pressure, equal to the mole fraction x_i multiplied by P, the total pressure, and the standard state is usually pure component i.

For an ideal solid solution, the same expression holds with p_i/p_i^o replaced by x_i/x_i^o. However, the standard state is pure i, so $x_i^o = 1$. The form of eq. (3) is so useful that it is retained even for non-ideal solutions with x_i replaced by the activity, a_i, which may also be considered a product of x_i multiplied by a non-ideality factor, γ_i, the activity coefficient.

Driving Force for Epitaxy

As an example, consider the OMVPE growth of GaAs using trimethylgallium (TMGa) and arsine (AsH_3). The overall reaction is,

$$\left(CH_3\right)_3 Ga(v) + AsH_3(v) = GaAs(s) \tag{4}$$

Assuming the TMGa and AsH_3 to completely decompose in the gas phase to give Ga and As_4, an assumption that may need to be revisited in terms of kinetics, depending on growth conditions, the reaction can be simplified:

$$Ga(v) + \tfrac{1}{4} As_4(v) = GaAs(s). \tag{5}$$

The equilibrium condition is

$$\mu_{Ga}^{v} + \tfrac{1}{4} \mu_{As_4}^{v} = \mu_{GaAs}^{s}, \tag{6}$$

or

$$\mu_{Ga}^{ov} + \tfrac{1}{4}\mu_{As_4}^{ov} + RTp_{Ga}^{e}\left(p_{As_4}^{e}\right)^{1/4} = \mu_{GaAs}^{os} + RT\ln a_{GaAs}, \tag{7}$$

where the superscript "e" denotes the equilibrium value of partial pressure. Thus,

$$a_{GaAs} / p_{Ga}^{e}\left(p_{As_4}^{e}\right)^{1/4} = K_{GaAs}, \tag{8}$$

where K is the equilibrium constant. This is the basic law of mass action.

When the system is not at equilibrium, the thermodynamic driving force to restore equilibrium is

$$\Delta\mu = \mu_{Ga}^{v} + \tfrac{1}{4}\mu_{As_4}^{v} - \mu_{GaAs}^{s}, \tag{9}$$

or

$$\Delta\mu = RT\ln\left(\frac{p_{Ga}p_{As_4}^{1/4}}{p_{Ga}^{e}\left(p_{As_4}^{e}\right)^{1/4}}\right). \tag{10}$$

This is the driving force for epitaxy. A situation is intentionally created where higher than equilibrium reactant vapor pressures drive the system to produce the GaAs solid desired. The maximum quantity of GaAs solid that can be produced is simply the amount (the supersaturation) that would establish equilibrium, and is thus fundamentally limited by thermodynamics and the total amount of gas transported through the OMVPE reactor.

For the OMVPE growth of GaAs using arsine and TMGa, the thermodynamic driving force at 1000 K is approximately 80 kcal/mol [6]. This is due to the instability of both arsine and TMGa at 1000 K. MBE and CBE also fall into the category of having a very high driving force, in this case, due to the instability of elemental Ga and As in the vapor at typical growth temperatures. These high driving forces for formation of the solid have prompted many researchers to dub OMVPE, MBE, and CBE as "highly non-equilibrium growth processes [1,6]. On the other hand, hydride and halide VPE have much smaller thermodynamic driving forces. They have been treated using equilibrium thermodynamics for decades [7].

This raises the question: How does thermodynamics relate to epitaxial growth for OMVPE and MBE, where the driving force is extremely high? Even for these processes, powerful thermodynamic forces still control much of the growth process. This is because, even for a system with a high supersaturation of the input vapor phase, near equilibrium conditions may prevail near the solid/vapor interface. This means that thermodynamics can provide important information about the growth process and the properties of the resultant materials. However, it may prove necessary to consider the thermodynamic properties of the surface in addition to the vapor and bulk solid phases. Thermodynamic factors largely determine the equilibrium structure of the surface, leading to surface phase diagrams, as discussed below, that give the surface reconstruction (bonding) as a function of the extensive parameters, such as temperature and the group V partial pressure, as discussed below. The surface

reconstruction has profound effects on both the epitaxial growth processes and the properties of the resulting layer.

Ordinarily, in the OMVPE system, the growth rate is considerably less than that calculated from thermodynamics. Kinetics, both surface reaction rates (at low temperatures) and diffusion through the gas phase (at higher temperatures), are not rapid enough to allow equilibrium to be established throughout the system at all times. This situation is illustrated by Fig. 1a, where $\Delta\mu$ from eq. (9) is plotted versus reaction coordinate. This allows the schematic representation of the overall, thermodynamic driving force for the growth reaction, represented as $\Delta\mu^*$. The superscript "* " denotes the chemical potential in the input gas phase, where for all reactants $p_i=p_i^*$. The growth rate is proportional to the flux of atoms diffusing through the boundary layer, which is identical to the flux of atoms crossing the interface into the solid. The diagram shows schematically the driving forces necessary to sustain this flux for the diffusion process ($\Delta\mu_D$) and the surface reactions ($\Delta\mu_S$).

Even in cases with a large supersaturation in the input vapor phase, i.e., $\Delta\mu^*>>0$, near equilibrium conditions may exist at the growing solid surface. This simply requires that the interface kinetics be much more rapid than the diffusion kinetics. Then, the two processes proceed at the same rate with $\Delta\mu_S<<\Delta\mu_D$. This situation, termed diffusion limited growth, is shown schematically in Fig. 1b. Using ordinary growth conditions, with temperatures between approximately 550 and 800 °C, this is the normal situation for the OMVPE growth of GaAs, as deduced from the nearly temperature independent growth rate [1].

Many of these features of OMVPE growth can be accurately described using this equilibrium approximation. However, it should be remembered that kinetic limitations (especially at low temperatures) can hinder the approach to equilibrium in some cases. An example is the incomplete decomposition of one of the reactants. In that case, kinetic factors will typically control the solid composition and growth rate. For such surface kinetically limited processes, the growth rate increases exponentially with increasing temperature [1,8]. This occurs for the OMVPE growth of GaAs at temperatures below approximately 550 °C when TMGa is the Ga precursor, but this temperature depends on the group III precursor used, since the temperatures required for complete pyrolysis of the precursor molecules depends on the bond strengths in the group III source molecules [1,6].

In the diffusion limited case, illustrated schematically in Fig. 1b, the interfacial partial pressures, p_i^i, nearly satisfy the equilibrium relationship,

$$\frac{a_{GaAs}}{p_{Ga}^i\left(p_{As_4}^i\right)^{1/4}} = K_{GaAs}\,. \tag{11}$$

Since the input vapor is highly supersaturated,

$$p_{Ga}^*\left(p_{As_4}^*\right)^{1/4} >> p_{Ga}^i\left(p_{As_4}^i\right)^{1/4}. \tag{12}$$

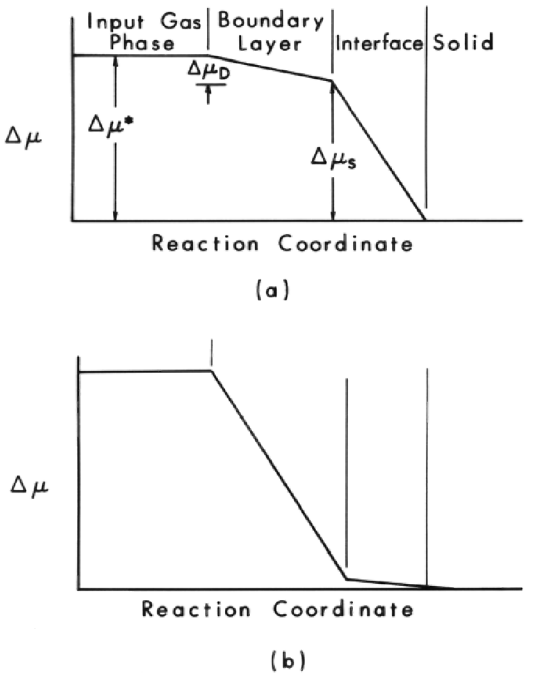

FIGURE 1. Diagram of chemical potential versus reaction coordinate, showing the drop in chemical potential required for driving diffusion (subscript D) and surface reactions (subscript S) to keep all rates equal: (a) general case, (b) rapid surface kinetics. (after Stringfellow [9]).

This is equivalent to stating that $\Delta\mu^* >> 0$. For the typical case

$$p^*_{Ga} << \tfrac{1}{4} p^*_{As_4}, \tag{13}$$

i.e., the V/III ratio is >>1. This means that the Ga is nearly depleted at the interface,

$$p^i_{Ga} << p^*_{Ga}, \tag{14}$$

while the As_4 partial pressure is hardly diminished,

$$p^i_{As_4} \approx p^*_{As_4}, \tag{15}$$

since the same number of As and Ga atoms are removed from the vapor phase to produce GaAs. This situation makes the analysis of growth rate and solid composition particularly simple.

The growth rate is proportional to the flux of Ga and As atoms diffusing through the vapor to the growing interface. For simplicity, this can be analyzed in terms of diffusion through a boundary layer of thickness d. A more complete description is

given in references [1,10]. The two fluxes are equal, since stoichiometric GaAs is the only product. The flux may be expressed,

$$J = D_{Ga}\left(p^{*}_{Ga} - p^{i}_{Ga}\right)/\,RTd\,, \tag{16}$$

where D_{Ga} is the diffusion coefficient of Ga, in whatever form it may appear while diffusing through the boundary layer. In light of eq. (14), the Ga flux and the GaAs growth rate are proportional to p^{*}_{Ga}, as observed experimentally [9]. Equally clear is that the ratio of the concentrations of A and B for alloys with mixing on the group III sublattice, $A_{1-x}B_xC$, will be the same as the ratio p^{*}_{A}/p^{*}_{B}, assuming the diffusion coefficients for the A and B species are nearly the same. Thus, the group III distribution coefficients are nearly unity for OMVPE growth [11]. This will, in general, not be true for growth in halide VPE systems [7].

For MBE growth, the situation is quite similar. The growth rate is typically determined by the rate of arrival of group III atoms at the solid-vapor interface [2]. The group V element is incorporated from the vapor in the amount needed to produce a stoichiometric III/V compound or alloy. Again, at low temperatures, where the group III atoms cannot re-evaporate from the growing surface, the ratio of the group III elements incorporated into the solid, for mixing on the group III sublattice, is the same as the ratio of the fluxes of the group III atoms to the surface. For both OMVPE and MBE, as the temperature is raised to the point that group III atoms can re-evaporate from the surface, thermodynamic factors begin to control the solid composition [11]. For mixing on the group V sublattice, thermodynamics typically controls the solid composition [11].

Solution Thermodynamics

The condition for thermodynamic equilibrium is expressed by eq. (1) as discussed above. Using these concepts, applied to the solid-vapor equilibria of concern for OMVPE, we can calculate the composition of a multicomponent solid alloy from the temperature and the concentrations of the various components in the vapor phase. Deviations from ideality for the vapor phase are commonly neglected. However, non-ideality in the solid phase must be considered. Fortunately, for semiconductor systems the solid can often be described using either the regular solution [12] or the "delta-lattice-parameter" (DLP) [13] model. In both cases the distribution of elements on a sublattice is considered to be random; thus, the entropy of mixing for a pseudobinary solution of the type $A_{1-x}B_xC$ is simply the ideal configurational entropy of mixing,

$$\Delta S^{M} = -R\left(x\ln x + (1-x)\ln(1-x)\right) \tag{17}$$

For the regular solution model, the enthalpy of mixing is obtained by summing nearest-neighbor bond energies, yielding,

$$\Delta H^M = x(1-x)\Omega^S, \tag{18}$$

where Ω^S is the interaction parameter. The activity coefficient may be written,

$$\ln \gamma_i = (1-x_i)^2 \Omega / RT. \tag{19}$$

Physically, the regular solution model cannot provide an accurate, predictive description of the enthalpy of mixing in semiconductor alloys. However, simple models developed to interpret the band gap and optical properties can be used to treat the bonding in semiconductor alloys [13]. The DLP model allows accurate calculation of Ω^S in terms of the difference in lattice parameters between AC and BC:

$$\Omega^S = 5 \times 10^7 (a_{AC} - a_{BC})^2 \left(\frac{a_{AC} + a_{BC}}{2} \right)^{-4.5}. \tag{20}$$

This first-order treatment of the enthalpy of mixing is apparently equivalent to considering only the microscopic bond strain energy caused by the lattice parameter difference [14]. In recent years the valence force field (VFF) model [15-17] as well as first principles calculations [18], giving accurate estimates of the enthalpy of mixing without adjustable parameters, have been developed. Using these approaches, we find that the solutions are nearly ideal ($\Omega^S = 0$) for alloys from compounds with the same lattice constant such as GaAs and AlAs, and to have positive deviations from ideality for all other alloys. The enthalpy of mixing increases with the square of the difference in lattice parameters of the two constituent compounds (or elements for group IV alloys) in the DLP model. This can overwhelm the negative configurational entropy of mixing for temperatures below the critical temperature, T_c, resulting in a free energy versus composition curve with an upward bowing in the center [19]. This dictates that at equilibrium a random alloy in a certain composition range will decompose into a mixture of two phases, i.e., the phase diagram contains a miscibility gap.

The equilibrium conditions for the ternary(or pseudobinary) system may be obtained in exactly the same way as described above for binary systems, by equating the chemical potentials of the 2 components in the 2 phases:

$$\begin{aligned} \mu_A^v + \mu_C^v &= \mu_{AC}^s \\ \mu_B^v + \mu_C^v &= \mu_{BC}^s \end{aligned} \tag{21 a and b}$$

This leads to two mass action expressions, similar to eq. (11). As discussed above, equilibrium is assumed to be established at the interface.

As an example of the use of such calculations to understand epitaxial processes, consider the OMVPE growth of $GaAs_{1-x}Sb_x$. The 2 mass action expressions, one for GaAs and one for GaSb, are solved simultaneously with 2 conservation equations, one for solid stoichiometry and one for solid composition [20]. Complete pyrolysis of

the source molecules is normally assumed. This assumption is incorrect for very stable molecules at all temperatures and for all molecules at very low temperatures. The activity coefficients of GaAs and GaSb in the solid are calculated as described above using the DLP model.

The calculation can be performed with no adjustable parameters, yielding solid composition versus vapor composition and substrate temperature during growth. The calculated results are compared with experimental data in Fig. 2 [21]. Several important aspects of VPE are illustrated in this rather complex figure. First, consider the open data points, obtained for an input V/III ratio (the ratio of the input group V to group III molar flow rates) of 2.0. Notice that the calculated curve for V/III = 2.0 fits the data well. The Sb distribution coefficient, defined as $k_{Sb}= x^{s}_{Sb}/x^{v}_{Sb}$, where $x^{v}_{Sb} = p^{*}_{TMSb}/(p^{*}_{TMSb}+p^{*}_{AsH3})$, is seen to be less than unity. GaAs is more stable than GaSb, thus As is more likely to bond to the Ga on the surface and be incorporated into the solid. The excess Sb evaporates from the surface.

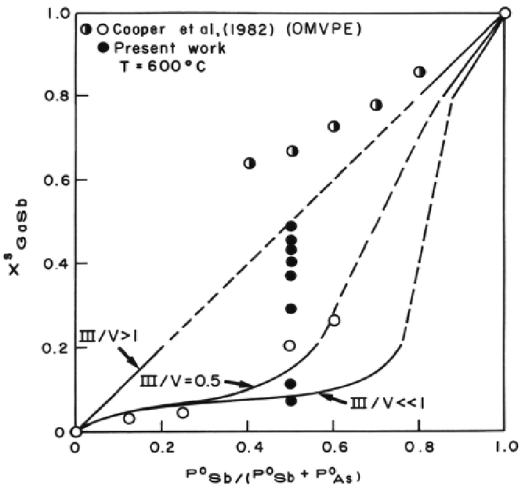

FIGURE 2. Solid versus vapor composition for the alloy GaAsSb. The curves were calculated for various V/III ratios. Broken sections represent calculated regions of solid immiscibility. (after Stringfellow and Cherng [21]).

An additional important point is that the calculation for a V/III ratio of less than unity yields an antimony distribution coefficient of unity. For the case of alloys with mixing on the group III sublattice, when V/III>1, essentially all of the group III elements reaching the interface are incorporated. The case of GaAsSb with mixing on the group V sublattice with V/III≤1 is completely analogous. The establishment of equilibrium at the interface while the input vapor is highly supersaturated requires that the group V elements be virtually exhausted at the interface. A final point relative to Fig. 2 is the presence of a two solid phase region or miscibility gap. Because of the large difference in lattice constant between GaAs and GaSb a miscibility gap exists [22]. However, when the V/III ratio is less than unity, the As and Sb atoms arriving

in a random pattern at the surface do not have time to redistribute themselves into GaAs and GaSb rich areas before being covered over by the next layer. Thus, we are able to grow metastable $GaAa_{1-x}Sb_x$ alloys throughout the entire range of solid composition as shown by the solid data points in Fig. 2.

Evidence of phase separation has been observed, even for commercially important alloys such as GaInAsP [20]. Even the important alloy GaInN, used for short wavelength LEDs and lasers, is predicted to have a significant miscibility gap, although the solubility of In in GaN is predicted to be 6% at 850°C [15]. This has led to wide-spread reports of the spontaneous formation of quantum dots in the quantum wells used in the active regions of these devices [23]. A recent, dramatic example of this phenomenon involves alloys where N, an extremely small group V element, is used to replace a much larger element such as As or P [24]. The amount of N that can be added, at equilibrium, is limited to values of much less than 1% [16,17].

Solid Phase Immiscibility

For GaAsSb, the value of T_C, the temperature above which the miscibility gap disappears, is approximately 745 °C [20]. At typical growth temperatures, the solid compositions inside the miscibility gap, which covers nearly the entire composition range, cannot be grown by liquid phase epitaxy (LPE) [25]. We have already discussed the ability to grow the metastable alloys by OMVPE. They can also be grown by molecular beam epitaxy (MBE) [26]. Recently, it has been discovered that these alloys may also exhibit an ordered, monolayer-superlattice structure [27], consisting, in the ideal case, of alternating monolayers of GaAs and GaSb.

Atomic-scale ordering in a thermodynamic system where the random alloy exhibits a large positive enthalpy of mixing is not thermodynamically stable for a regular solution [12]. However, such ordering is widely observed in alloys involving group IV, III/V, and II/VI semiconductors [28]. Ordering has now been observed in essentially all III/V alloys grown by OMVPE and MBE [11,28]. The {111} ordered structure (Cu-Pt) with 4 variants, corresponding to the 4 crystallographically distinct {111} planes in a cubic lattice, is normally observed for III/V alloys. Only 2 of the variants are observed during OMVPE growth for (001)-oriented substrates. This is apparently due to the lower symmetry of the reconstructed, As-rich surface.

The occurrence and mechanism of ordering are fascinating materials science problems that reveal much about the thermodynamics and structure-property relationships for semiconductor alloys. They also reveal important general features of the surface processes occurring during vapor phase epitaxial growth. This topic is discussed in more detail below.

Surface Phase Diagrams

Clearly, the surface structure plays such an important role in the OMVPE growth process and the properties of the resulting epitaxial layers. Since this topic is perhaps the least understood and most rapidly advancing fundamental aspect of OMVPE, it will be reviewed in more detail in what follows.

The unreconstructed (001) surface of a diamond cubic or zincblende semiconductor has 2 dangling bonds per atom. This suggests that a reconstruction of the bonding at the surface would significantly lower the free energy. The tetragonal geometry of covalent sp^3 bonds on a group V rich surface, combined with the propensity of these atoms to form dimers in the vapor, suggests the formation of dimer bonds on the surface. Generally reliable estimates of the surface bonding and reconstruction come from the so-called "electron counting" rule [29]. This has led to several proposed stable reconstructions. The first experimental evidence came from *in situ* electron diffraction during MBE growth [30]. The development of *in situ* tools for observing the surface during OMVPE growth has been much slower because a blanket of hydrogen or nitrogen is typically present over the growing surface which attenuates the electron beam.

The development of optical techniques such as reflection difference spectroscopy (RDS) [31], surface photo absorption (SPA) [32], and scanning tunneling microscopy (STM) [33] has allowed the clarification of the surface during OMVPE growth. The results of these studies indicate that the surface reconstruction during OMVPE growth of (001) GaAs is the As-rich (2x4) reconstruction [34,35]. For the phosphides, the (2x2) reconstruction is stable. It consists of a complete coverage of the surface by P dimers, with the electron counting rule satisfied by an H attached to each P dimmer [33]. The surface phase diagram specifies the equilibrium surface reconstruction as a function of extensive thermodynamic parameters, typically temperature and the group V partial pressure. These stable (001) surfaces give rise to high surface mobilities for adsorbed atoms, with diffusion lengths as large as a micron [36]. This is the key to obtaining the nearly atomically abrupt interfaces reported for the OMVPE and MBE growth of quantum well structures widely reported in the literature. Ad-atoms that could make two bonds to the surface atoms would obviously not be mobile. This would lead to statistically rough, three dimensional growth, precluding the possibility of producing quantum wells and other nano-structures.

A dramatic effect of the surface reconstruction observed for III/V semiconductors grown by OMVPE relates to the microstructure of alloys. As indicated above, the DLP model predicts that the enthalpy of mixing of III/V alloys is always positive. This means that we expect the alloys to evidence clustering and phase separation and that ordering should not be observed [12,37]. However, TEM investigations of many III/V alloys indicate that ordered structures are formed spontaneously during OMVPE growth [28]. In particular, the CuPt structure, with ordering on the {111} planes, is observed in most III/V alloys, including GaInP. The formation of this ordered structure is extremely significant, because it markedly reduces the bandgap energy. Bandgap differences as large as 160 meV between partially ordered and disordered materials have been reported for GaInP [38]. The order parameter can be directly linked to the surface SPA spectrum measured *in situ* during growth. The change in order parameter induced by changes in the temperature and the partial pressure of the P precursor during growth is linearly related to the magnitude of the SPA signal at 405 nm due to the P dimers characteristic of the surface [28].

A powerful tool for controlling the surface bonding and structure during OMVPE growth is the use of surfactants. Surfactants, in this context, are elements that accumulate at the surface during growth. For example, adding a small amount of an

Sb precursor, such as TESb, during the OMVPE growth of GaInP results in the displacement of some surface P dimers by larger Sb dimers. This is indicated directly by the SPA spectra [28] supported by the results of first principles calculations[39]. The Sb is rejected from the solid due to its' large size (relative to P) and does not leave the surface rapidly by evaporation due to its relatively low volatility. Sb is a perfect surfactant since it does not act to dope the III/V semiconductors, since it is, itself, a group V element.

The effect of a small concentration of the Sb precursor, TESb, on the degree of order of GaInP lattice matched to GaAs is shown in Fig. 3 [40]. The TESb partial pressure is normalized by the total group III precursor partial pressure, since both Sb and the group III elements are relatively non-volatile, although the Sb distribution coefficient is measured to be <<1, presumably due to SbH_3 desorption from the surface [41]. The degree of CuPt order is clearly decreased as Sb is added to the surface. This is not a bulk effect, since the mole fraction of Sb incorporated into the solid, determined from SIMS analysis, is only approximately $5x10^{-5}$ (or 10^{18} cm^{-3}) for an Sb/III ratio in the vapor of $2x10^{-2}$.

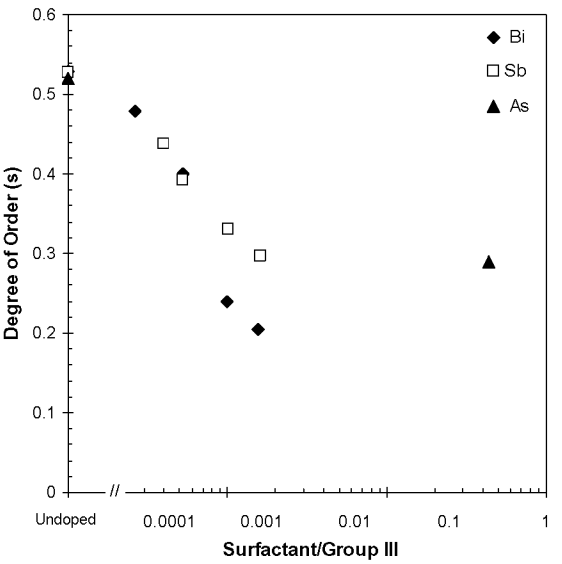

FIGURE 3. Degree of order for GaInP layers grown by OMVPE plotted versus the surfactant/III ratio in the vapor. Data are for Bi (♦), Sb (□), and As (▲). (After Stringfellow *et al.* [40].)

SPA anisotropy spectra for various Sb/P concentrations in the vapor lead to a correlation of the decrease in order parameter with a decrease in the magnitude of the SPA signal at 405 nm due to [$1\bar{1}0$] P dimers [28]. This suggests that the reduction in order parameter occurs due to the elimination of the P dimers, which are predicted to provide the driving force for CuPt ordering. This is most likely due to direct replacement of the [$1\bar{1}0$] P dimers by Sb dimers with the same orientation. This is

verified by recent first principle calculations for [39,42]. For small Sb coverage of the surface, the lowest energy configuration is for Sb to substitute directly for at the surface. This results in the observed reduction in degree of order produced by Sb addition to the system. The larger spacing of the Sb dimers gives a smaller amount of strain in the subsurface layers, resulting in a reduced thermodynamic driving force for CuPt ordering. This phenomenon is of extreme technological significance. The use of Sb (or Bi) is an efficient and convenient method for removing ordering, and hence increasing the bandgap energy, for LED and solar cell devices. In fact, to obtain the highest solar cell efficiencies, the GaInP in cascade solar cells must be disordered [43]. This is conveniently accomplished by the use of surfactant Sb during OMVPE growth [43]. The presence of Sb during growth also leads to a reduction in defect densities in lattice mismatched solar cell structure [44].

The SPA spectrum at larger Sb/III ratios in the vapor is seen to be distinctly different, indicative of formation of a non-(2x4)-like structure [45]. TED patterns of the material produced using this TESb concentration indicate that the A variants of a triple-period ordered (TPO) structure are formed [45]. The first principles calculations of Wixom et al. [39] indicate that (4x3) or (2x3) reconstructions will form at higher Sb surface concentrations. This would stabilize the A variants of the TPO structure. This was the first report of the use of a surfactant to change the ordered structure by changing the surface reconstruction [46].

The surfactant effect of Sb on Cu-Pt ordering can be used to modulate the bandgap energy during growth by varying the TESb flow rate to produce unique heterostructures where the composition of all layers is identical [47]. The 20-K PL data clearly show that the difference in bandgap energy is 135 meV [47]. This technique has also been used to produce double heterostructures and quantum wells with well layers as thin as 6.7 nm [47,48,49].

From these results it is clear that a small concentration of TESb, added during OMVPE growth, can be used to modify the surface reconstruction. This leads to a marked change in the microstructure and, hence, the semiconducting properties of the solid. Other group V surfactants, isoelectronic with P, have similar effects. For As (from the pyrolysis of TEAs) rejection from the solid is much less than for Sb due to the decreased size difference relative to the host P [13,37]. It is also more volatile than Sb. Thus, it is expected to have less of a surfactant effect. Indeed, at low ratios of TEAs to phosphine in the vapor, both PL and TEM analysis indicate that the layers are highly ordered. However, TEM results show that $(As/III)_v = 0.45$ produces a significant reduction in the order parameter, as shown in Fig. 3. SPA spectra show a clear decrease in intensity at 405 nm [46] indicating that, as for Sb, the decrease in CuPt ordering is due to displacement of the $[1\bar{1}0]$ P dimers that drive the CuPt ordering process.

Bi is the largest of the surfactants isoelectronic with P and is, thus, much more difficult to incorporate into the solid [13,37]. It is also the least volatile of the group V surfactants studied. The order parameters deduced from the 20K PL peak energies for GaInP layers lattice matched to GaAs grown with several ratios of Bi/III in the vapor are shown in Fig. 3. The addition of Bi results in a decrease in the order parameter similar to that seen for Sb [50]. This is supported by TEM results. The SPA spectrum

is changed markedly when sufficient Bi is added to the system to cause disordering [50].

These results confirm that the group V elements larger than P (As, Sb, and Bi) all give reduced strain in the subsurface GaInP layers, leading to a reduction in the thermodynamic driving force for CuPt ordering. Another group V surfactant, N, is *smaller* than P and so has the potential to *increase* the subsurface strain, if, indeed, $[\bar{1}10]$ N dimers are formed on the surface. Sb and Bi are obvious choices as surfactants, since they are rejected from the solid and have low vapor pressures, so are expected to accumulate at the surface. N will also be rejected from the solid, as known from the results of previous thermodynamic calculations [13,17,37], but it is much more volatile than P. However, the As results indicate that even relatively volatile group V elements can be effective surfactants. For N, high partial pressures of a relatively labile precursor are required to obtain a significant N coverage of the surface. In fact, a change in surface reconstruction using N during MBE growth has been reported for GaAs [51]. This leads one to expect significant N surface coverages during the OMVPE growth of GaInP under suitable conditions, i.e., low temperatures and high N/P ratios in the vapor.

The experimental results obtained using DMHy as the N precursor at 620°C on singular GaAs substrates with DMHy/TBP ratios as high as 0.8 indicate a clear decrease in order parameter [52]. *In situ* SPA results indicate a decrease in the 405 nm peak due to P dimers. The results were interpreted as indicating that N does, indeed, replace P on the surface. However, the decrease in order parameter may indicate that N dimers do not form. This may be due to the large strain energy required to form N dimers on the GaInP surface and is consistent with previous work of N on GaN surfaces, where N-dimers are not formed [53].

Another striking effect of surfactants added during OMVPE growth is the change in incorporation coefficients of dopants and alloying elements. Surfactants isoelectronic with As were first demonstrated to significantly affect dopant incorporation in GaAs. Three layer Zn and In doped structures were grown with TESb added only in the middle layer. The results show that addition of Sb leads to an increase in both the Zn and In concentrations [54]. For a small amount of TESb in the vapor (Sb/III=0.012) the Zn concentration in the layer increased sharply by 60%. The Sb concentration in the layers was very small ($2–3\times10^{17}$ atoms/cm^3). After the TESb was removed from the vapor, as indicated by a decrease in the Sb concentration in the epilayer, the Zn concentration decreased as well. The correlation between the change in the Zn and Sb concentrations in the layer clearly indicated that surface Sb increases the incorporation of Zn in GaAs. The SIMS depth profile of a GaAs epilayer that was inadvertently doped with In showed a similar correlation between an increase in the In and the presence of Sb during growth [54]. The concentration of P inadvertently present in the GaAs epilayers was also measured. Apparently, Sb had little affect on the concentration of P, which is incorporated on group V sites. The results were interpreted in terms of either an Sb-induced increased group III adatom surface diffusion coefficient or an increase in the group III sticking coefficient at the step edge induced by Sb. Either would cause an increase in In and Zn incorporation into the GaAs, but would have no affect on P incorporation [54].

More recent studies [55, 56] have clearly demonstrated even more pronounced effects of Sb on Zn doping in GaP. As seen in Fig. 4 [56], the increase in Zn doping due to surfactant Sb can be as large as a factor of 10. Of perhaps equal significance is the discovery that the Sb (Bi has been observed to have a similar effect) also reduces the concentration of residual background C. In Fig. 4, the carbon concentration is reduced to below the SIMS detectability limit. In a sample grown at a higher temperature, where the background C concentration is much higher, the Sb was found to reduce C by a factor of >100. Both of these effects are likely to be technologically valuable [56].

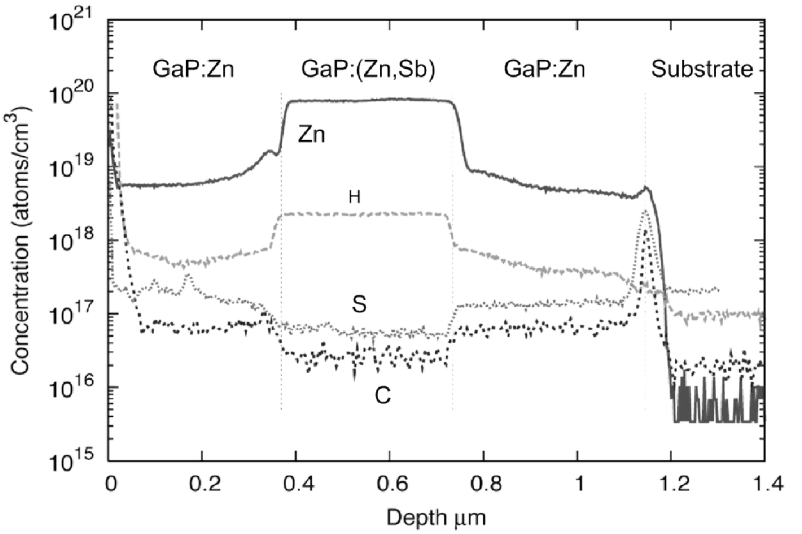

FIGURE 4. SIMS profile of Zn doped GaP epilayer grown at 650 C, with Sb added only during growth of the middle layer of the 3 layer structure. (After Howard *et al* [56].)

KINETICS

The kinetics of OMVPE reactions are extremely complex; thus, even today, our understanding is incomplete. Gas phase reactions include the pyrolysis reactions yielding the components of the epitaxial layer, as well as complex reactions involving adduct formation in the vapor, due to the Lewis acid and Lewis base natures of many of the respective group III and group V precursor molecules. As a further complication, the gas phase pyrolysis reactions are seldom complete, so heterogeneous pyrolysis reactions occurring on the growing surface often play a key role in the pyrolysis and growth reactions [1,10].

The reaction kinetics are closely linked to the hydrodynamic and mass transport aspects of the OMVPE growth process, which further complicates the analysis and understanding of these processes. First principles calculations are frequently used to help sort out these complex problems. This topic is treated in some detail in the

literature [10] so will not be treated further here. Such calculations are often used as an aid in reactor design and are expected to become even more useful as we unravel the complexities of the homogeneous and heterogeneous chemical reactions occurring during deposition.

Since heterogeneous pyrolysis reactions are often an important part of the overall OMVPE growth process, it is expected that the chemical and physical state of the surface will have an important role. This is a topic that is somewhat neglected. Nevertheless, it is clear that surface reconstruction, as controlled by the temperature and gas phase composition as well as the presence of surfactants will play an essential role in the overall kinetics of the growth process.

Processes Occurring at the Surface

The basic physical processes occurring at the surface during epitaxial growth have been generally known for many decades [57,58]. The surface during growth, and indeed at equilibrium, is seen to be somewhat rough due to entropic effects, with steps, adatoms, advacancies, etc. The adatoms and advacancies can condense into 2 dimensional clusters. The steps, themselves, may also be rough due to the presence of kinks. Growth occurs by the propagation of steps as well as by the formation and propagation of 2 dimensional and 3 dimensional islands. Of course, the tools necessary to actually see the features and follow the step motion and nucleation during growth were missing until recently.

Today, for the first time, we are able to resolve all of these surface features for semiconductor materials using scanning probe microscopy techniques [59,60]. The STM can be used to directly image the surface atoms to determine the surface reconstruction in Si [60] and in GaAs [61]. Individual adatoms and islands can also be viewed using the STM, as well as the advacancies and advacancy clusters.

The first item of discussion must, of course, be the bonding at the surface during growth. The surface reconstruction, which has been discussed above, is observed to be virtually the same as for the static surface; thus, it is given by the surface phase diagram. It is a function of growth parameters such as temperature and V/III ratio as well as the activity of H in the system. The reconstruction has a first order effect on all of the phenomena to be discussed below. It is also expected that the surface reconstruction will affect the chemical processes occurring at the surface such as adsorption/desorption and surface reactions.

The steps and kinks on the reconstructed surfaces can be easily viewed by STM for both Si and GaAs surfaces [60,62]. For (001) Si surfaces the steps parallel and perpendicular to the rows of Si dimers are smooth and rough, respectively, because adatom attachment at steps is much more likely at the ends of the [110] dimer rows [60]. For the conditions used for epitaxial growth, (001) GaAs surfaces typically consist entirely of As terminated terraces. Thus, the III/V steps are the equivalent of 2 steps on the Si surface. Such steps are typically referred to as monolayer, even though they have a height of 1/2 the lattice constant.

Simple models have been postulated for the attachment of adatoms at step edges on the (001) GaAs surface. Asai [63] studied the growth of macroscopic islands produced photolithographically on the surface. The islands were found to change

shape during OMVPE growth, due to the difference in propagation rate for the two orthogonal <110> steps. At high As partial pressures, the rate of propagation of the $[\bar{1}10]$ steps was found to be higher than for [110] steps. This was attributed to the higher adatom sticking coefficient at the $[\bar{1}10]$ steps, where 3 bonds are made to the Ga adatom at the step edge when the As coverage is high. Only 2 bonds are formed for the Ga adatom attaching itself at the [110] steps. This simple model, which neglects reconstruction on the surface and at the step edge, qualitatively describes quite well the effects of temperature and AsH_3 flow rate on the island shape.

The configuration of the surface during growth depends on the step density, the sticking coefficient at the step edge, and the flux of adatoms to the surface. For vicinal substrates where the surface is covered by an array of steps induced by the misorientation, growth frequently occurs via step flow growth. In this case, each adatom has the time and mobility to diffuse to a step where it is incorporated into the solid. In the case where the step spacing is too large or the diffusion coefficient too small, the supersaturation builds up between steps. When it is large enough it causes nucleation of a new 2 dimensional island between existing steps. This results in the type of 2 dimensional nucleation and growth (layer-by-layer growth) that is virtually always observed for singular (001) substrates.

The steps formed during epitaxial growth are frequently found not to be monolayers. For unstrained layers, the steps are expected to have a mild repulsion[64]. This suggests that the step structure, itself, can be different for the monolayer and bilayer steps. Some growth conditions lead to the formation of even larger steps, from approximately 10 to 50Å in height, for layers of both GaAs [65] and GaInP [66] grown by OMVPE on vicinal surfaces. For layers grown by OMVPE, the size and separation of the bunched steps (supersteps) are found to depend on the growth conditions. The formation of supersteps is nearly eliminated as the temperature was raised to 720 °C [66]. Superstep height is also found to decrease with increasing growth rate in both GaAs [67] and GaInP [66]. This type of step bunching is also found to occur at the edges of islands formed on singular substrates.

The origin of step bunching has been variously attributed to thermodynamic and kinetic factors. Step bunching on vicinal surfaces can be considered thermodynamically in terms of simple phase separation. At high temperatures, where entropy is the dominant term in the free energy, an array of individual steps has the lowest free energy, since the entropy of a set of individual steps is higher than when the steps are collected together to form a facet. If low surface energy facets can form, they will "precipitate" as the temperature is lowered [4]. The other, extremely important factor is the change in the nature of the surface structures on both the terraces and bunched step edges, i.e., the facets, as the temperature is varied. A third consideration is strain. Long range attractive forces between steps exist in strained epitaxial layers that are absent in unstrained layers [64]. Together, these considerations allow, in principle, the construction of a surface phase diagram that includes facets, steps, and singular terraces.

Kinetic factors can also led to step instability, i.e., the collection of monolayer steps together to form supersteps. A simple example illustrates this effect. It is likely that

the sticking coefficient for an adatom approaching a step edge will be different when the approach is from the lower terrace (an up step) than from the upper terrace (a down step). It has been suggested that an atatom arriving at a down step will face an extra energy barrier because the bonding cannot be maintained as the adatom passes over the step. The presence of this "Schwoebel" barrier [68] would result in a higher sticking coefficient for an adatom approaching the step from the lower terrace than from the upper terrace. If the sticking coefficient is, indeed, higher from the lower terrace, the shorter terraces will become longer and the longer terraces shorter. This will, of course, lead to step ordering, i.e., the kinetics will favor formation of a structure with a uniform spacing of monolayer steps [69]. If the ratio the sticking coefficients is reversed, with an adatom more likely to stick at a down step, the steps will bunch together.

For growth on singular substrates, the presence of Schwoebel barriers at the step edges makes it difficult for atoms arriving on top of an existing nucleus to move to the lower terrace. This results in a form of kinetic roughening of the surface where the islands on the surface form 3 dimensionsal "wedding cake" like structures. The presence of the barrier makes the steps uniformly spaced at the island edges [69]. Amazingly, the features observed on these tiny islands formed naturally during OMVPE growth [70] mimic nearly exactly the features observed for macroscopic islands[63]. For example, the island asymmetry, due to the difference in sticking coefficients of adatoms at $[\bar{1}10]$ and [110] steps, changes with temperature and the partial pressure of the P precursor in ways that are nearly identical to those observed by Asai [63].

Kinetic roughening can also occur when the sticking coefficient of adatoms is high and the surface mobility is low. Naturally, this "statistical roughening" becomes greater as the layer thickness increases [4].

Another factor leading to roughening in heteroepitaxial systems is basically thermodynamic. When a thin epitaxial layer is grown on a highly mismatched substrate, it will elastically deform, like a drum head, to match the atom positions in the substrate. This creates a strain energy that increases approximately linearly with increasing epilayer thickness. As the layer gets thicker, the energy of the system can be reduced if the system separates into regions with thin epitaxial layers and small regions (islands) where the strain energy is relaxed by the formation of edge dislocations at the interface. Islands are formed since the dislocation energy is proportional to the area of the strain-relaxed, dislocated regions so the area of these regions is small. This is termed the Stranski-Krastanov growth mode [4].

Effects of Surface on Growth Processes

Studies of the detailed structure of the surface during epitaxial growth are not entirely academic. The physical nature of the surface, as described above, has significant consequences for epitaxial growth phenomena. For example, the surface structure affects adsorption/desorption phenomena. Naturally, the surface reconstruction affects the binding of adatoms at the surface and, hence, the adsorption energy. Thus, it will affect both adsorption/desorption rates as well as heterogeneous

reaction rates. Special sites, such as step edges, may also affect desorption. Furthermore, chemical reactions at these special sites may be higher than on the terraces. The surface structure, both the reconstruction and the step structure, is also expected to affect the mobility of adsorbed atoms and intermediate species on the surface.

SUMMARY

This chapter has discussed the fundamental aspects of vapor phase epitaxial growth, including the thermodynamic and kinetic aspects of the overall process. The emphasis has been on recent developments, many of which relate to the effects of the surface. The recent developments in understanding surface thermodynamics and the atomic scale physical processes occurring at the surface during growth have been facilitated by the recent development of a number of new tools for characterization of the surface *in-situ* during growth experiments. The surface atoms are found to reconstruct during vapor phase growth. The structures formed are found to be virtually the same as those formed at equilibrium, dependent on temperature, V/III ratio, and H chemical potential in the system. Thus, the bonding at the surface appears to be determined largely by thermodynamic factors. The experimental evidence supports a picture where the reconstructed surface is covered by an array of "defects" such as steps, kinks, adatoms, 2 dimesional adatom clusters, advacancies, and advacancy clusters. The surface reconstruction of the surface has profound effects on the OMVPE growth process. The bonding between the precursors and the surface has a first order dependence on the surface structure. Thus, the heterogeneous pyrolysis rates of both group III and group V precursors will depend on the surface. This determines, in part, the growth rate, solid composition, and incorporation of impurities dopants. In addition, the surface structure is found to have a direct effect on the microstructure of the semiconductor solid being grown. A well-understood example is the long range order exhibited by virtually all semiconductor alloys. The formation of the CuPt structure is driven by the surface construction.

ACKNOWLEDGMENTS

The author wishes to acknowledge the support of the Department of Energy through the Office of Basic Energy Science for long term support of the work discussed in this paper.

REFERENCES

1. G. B. Stringfellow, *Organometallic Vapor Phase Epitaxy: Theory and Practice*, 2nd Edition (Academic Press, San Diego, 1999).
2. M. A. Herman and H. Sitter, *Molecular Beam Epitaxy: Fundamentals and Current Status*, (Springer-Verlag, Berlin, 1989).
3. C. T. Foxon in *Handbook of Crystal Growth*, Vol. 3b, Thin Films and Epitaxy: Growth Mechanisms and Dynamics, ed. D.T.J. Hurle (Elsevier, Amsterdam, 1994).
4. J. Y. Tsao, In *Materials Fundamentals of Molecular Beam Epitaxy (*Academic Press, Boston, 1993).

5. D. T. J. Hurle (ed) *Handbook of Crystal Growth*, Vol. 3b,Thin Films and Epitaxy: Growth Mechanisms and Dynamics (Elsevier, Amsterdam, 1994).
6. G. B. Stringfellow, J. Crystal Growth **115,** 1 (1992).
7. J. B. Mullin and D. T. J. Hurle, J. Luminescence **7,** 176 (1973); A. Koukitu and H. Seki, Japan. J. Appl. Phys. **23**, 74 (1984).
8. D. W. Shaw, *Treatise on Solid State Chemistry*, Vol 5, ed., N. B. Hannay (Plenum, New York, 1975) p. 283.
9. G. B. Stringfellow, J. Cryst. Growth **68**, 111 (1984).
10. K. F. Jensen in *Handbook of Crystal Growth*, Vol. 3b, Thin Films and Epitaxy: Growth Mechanisms and Dynamics, ed. D.T.J. Hurle (Elsevier, Amsterdam, 1994).
11. See Ref. 1, Chapter 2.
12. R. A. Swalin, *Thermodynamics of Solids* (John Wiley and Sons, New York, 1962).
13. G. B. Stringfellow, J. Crystal Growth **27,** 21 (1974).
14. G. B. Stringfellow, J. Crystal Growth **98**, 108 (1989).
15. I. H. Ho and G. B. Stringfellow, *Appl. Phys. Lett.,* **69,** 2701 (1996).
16. I. H. Ho and G. B. Stringfellow, *of MRS,* **449,** 871 (1996).
17. I. H. Ho and G. B. Stringfellow, *J. Cryst. Growth.,* **178**, 1 (1997).
18. S. H. Wei and A. Zunger, *Phys. Rev. B,* **39,** 3279 (1989).
19. G. B. Stringfellow, *J. Crystal Growth,* **65,** 454 (1983).
20. G. B. Stringfellow, J. Crystal Growth **62,** 225 (1983).
21. G. B. Stringfellow and M. J. Cherng, J. Crystal Growth **64,** 413 (1983).
22. M. J. Cherng, R. M. Cohen and G. B. Stringfellow, J. Electron. Mater. **13**, 799 (1984).
23. Z. Liliental-Weber, D.N. Zakharov, K. M. Yu, J. W. Ager, W. Walukiewicz, E. E. Haller, H. Lu, and W. J. Schaff, J. Electron. Microscopy **54**, 243 (2005).
24. Y. C. Kao, T. P. Broekaert, H. Y. Liu, S. Tang, I. H. Ho, and G. B. Stringfellow, *Mat. Res. Soc. Symp. Proc.,* **423,** 335 (1996).
25. J. R. Pessetto and G. B. Stringfellow, J. Crystal Growth **62**,1 (1983).
26. J. Waho, S. Ogawa and S. Maruyama, Japan. J. Appl. Phys. **16,** 1875 (1977).
27. H. R. Jen, M. J. Cherng, and G. B. Stringfellow, Applied Physics Letters **48,** 1603 (1986).
28. G. B. Stringfellow, in *Spontaneous Ordering in Semiconductor Alloys*, ed. A. Mascarenhas (Kluwer Academic/Plenum Publishers, New York, 2002), Chapter 3.
29. M. D. Pashley, Phys. Rev. B **40**, 10481(1989).
30. H. H. Farrel and C. J. Palmstrom, J. Vac. Sci. Technol. **B8**, 903(1990).
31. D. E. Aspnes *et al*, J. Crystal Growth **120**, 71(1992).
32. N. Kobayashi, Y. Kobayashi, and K. Uwai, J. Crystal Growth **174**, 544 (1997).
33. L. Li, B. K. Han. D. Law, C. H. Li, Q. Fu, and R. F. Hicks, Appl. Phys. Lett. **75**, 683 (1999).
34. See Ref. 1, Chapter 3.
35. I. Kamiya, H. Tanaka, D. E. Aspnes, L. T. Florez, E. Colas, J. P. Harbison, and R. Bhat, Appl. Phys. Lett. **60**, 1238 (1992).
36. T. Isu, , M. Hata, Y. Morishita, Y. Nomura, and Y. Katayama, *J. Crystal Growth,* **115,** 423 (1991).
37. G. B. Stringfellow, Materials Science and Engineering **B87**, 97-116 (2001).
38. L. C. Su, I. H. Ho, N. Kobayashi, and G. B. Stringfellow, J. Crystal Growth **145**, 140 (1994).
39. R. R. Wixom, G. B. Stringfellow, and N. A. Modine, Phys. Rev., B **64**, 201322 (2001).
40. G. B. Stringfellow, J. K. Shurtleff, R. T. Lee, C. M. Fetzer, and S. W. Jun, J. Cryst. Growth, **221**, 1 (2000).
41. A. Howard and G. B. Stringfellow, J. Appl. Phys. (submitted)
42. R. R. Wixom, G. B. Stringfellow, and N. A. Modine, Phys. Rev. B **67**, 115309 (2003).
43. C. M. Fetzer, J. H. Ermer, R. R. King, and P. C. Cotler, U.S. Patent #7,126,052.
44. C. M. Fetzer, J. H. Ermer, R. R. King, and P. C. Cotler, U.S. Patent #7,122,734.
45. C. M. Fetzer, R. T. Lee, J. K. Shurtleff, G. B. Stringfellow, S. M. Lee, and T. Y. Seong, Appl. Phys. Lett., **76**, 1440 (2000).
46. G. B. Stringfellow, C. M. Fetzer, R. T. Lee, S. W. Jun, and J. K. Shurtleff, **583** MRS Symposium Proceedings p. 261 (2000).
47. R. T. Lee, J. K. Shurtleff, C. M. Fetzer, G. B. Stringfellow, S. Lee, and T. Y. Seong, J. Crystal Growth, **234**, 327 (2002).

48. J. K. Shurtleff, R.T. Lee, C. M. Fetzer, and G. B. Stringfellow, Appl. Phys. Lett. **75**, 1914 (1999).
49. G. B. Stringfellow, R.T. Lee, C. M. Fetzer, J. K. Shurtleff, Yu Hsu, S.W. Jun, S. Lee, and T.Y. Seong, J. Electron. Mater., **29**, 134 (2000).
50. S. W. Jun, R. T. Lee, C. M. Fetzer, J. K. Shurtleff, G. B. Stringfellow, C. S. Choi, and T. Y. Seong, J. Appl. Phys. **88**, 4429 (2000).
51. J. Lu, D. I. Westwood, L. Haworth, P. Hill, and J. E. Macdonald, Thin Solid Films **567,** 343-344 (1999).
52. D. Chapman, L. W. Rieth, G. B. Stringfellow, J. W. Lee, and T. Y. Seong , J. Appl. Phys. **95**, 6145 (2004)..
53. A. D. Bykhovski and M. S. Shur, Appl. Phys. Lett. **69**, 2397(1996).
54. J. K. Shurtleff, S. W. Jun, and G. B. Stringfellow, Appl. Phys. Lett. **78**, 3038 (2001).
55. D. C. Chapman, A. D. Howard, and G. B. Stringfellow, J. Crystal Growth **287**, 647 (2006).
56. A. D. Howard, D. C. Chapman, and G. B. Stringfellow, J. Appl. Phys. **100**, 44904 (2006).
57. W. Kossel, Nachr. Ges. Wiss. Gottingen, 135 (1927).
58. I. N. Stranski, Z. Phys. Chem., **136,** 259 (1928).
59. R. J. Hamers, U. K. Kohler, and J. E. Demuth, J. Vac. Sci. Tech, **A8,** 195 (1990).
60. M. G. Lagally, Y. W. Mo, R. Kariotis, B. S. Swartzentruber, and M. B. Webb, In *Kinetics of Ordering and Growth at Surfaces* (Ed, M. G. Lagally, 1990).
61. M. D. Pashley, K. W. Haberern, W. Friday, J. M. Woodall, and P. D. Kirchner, Phys. Rev. Lett. **60,** 217(1988).
62. B. G. Orr, J. Sudijono, and M. D. Johnson, *Mat. Res. Symp. Proc.,* **312,** 15 (1993).
63. H. Asai, J. Crystal Growth **80,** 425 (1987).
64. J. Tersoff, Y. H. Phang, Z. Zhang, and M. G. Lagally, Phys. Rev. Lett. **75,** 2730 (1995).
65. M. Kasu and N. Kobayashi, Appl. Phys. Lett. **62,** 1262 (1993).
66. G. B. Stringfellow and L. C. Su, J. Crystal Growth **163,** 128 (1996).
67. J. Ishizaki, S. Gota, M. Kishida, T. Fukui, T. and H. Hasegawa, Jpn. J. Appl. Phys. **33,** 721 (1994).
68. R. L. Schwoebel, J. Appl. Phys. **40,** 614 (1969).
69. C. Orme, M. D. Johnson, K. T. Leung, B. G. Orr, P. Smilauer, and D. Vvedensky, J. Crystal Growth **150,** 128 (1995).
70. R.T. Lee and G.B. Stringfellow, J. Appl. Phys. **83**, 3620 (1998).